ASTROBIOLOGY
Volume 21, Number 6, 2021
Mary Ann Liebert, Inc.
DOI: 10.1089/ast.2020.2344

Research Articles

Quantifying Preservation Potential: Lipid Degradation in a Mars-Analog Circumneutral Iron Deposit

Jonathan S.W. Tan and Mark A. Sephton

Abstract

Comparisons between the preservation potential of Mars-analog environments have historically been qualitative rather than quantitative. Recently, however, laboratory-based artificial maturation combined with kinetic modeling techniques have emerged as a potential means by which the preservation potential of solvent-soluble organic matter can be quantified in various Mars-analog environments. These methods consider how elevated temperatures, pressures, and organic–inorganic interactions influence the degradation of organic biomarkers post-burial. We used these techniques to investigate the preservation potential of deposits from a circumneutral iron-rich groundwater system. These deposits are composed of ferrihydrite ($Fe_5HO_8 \cdot 4H_2O$), an amorphous iron hydroxide mineral that is a common constituent of rocks found in ancient lacustrine environments on Mars, such as those observed in Gale Crater. Both natural and synthetic ferrihydrite samples were subjected to hydrous pyrolysis to observe the effects of long-term burial on the mineralogy and organic content of the samples. Our experiments revealed that organic–inorganic interactions in the samples are dominated by the transformation of iron minerals. As amorphous ferrihydrite transforms into more crystalline species, the decrease in surface area results in the desorption of organic matter, potentially rendering them more susceptible to degradation. We also find that circumneutral iron-rich deposits provide unfavorable conditions for the preservation of solvent-soluble organic matter. Quantitative comparisons between preservation potentials as calculated when using kinetic parameters show that circumneutral iron-rich deposits are $\sim$25 times less likely to preserve solvent-soluble organic matter compared with acidic, iron-rich environments. Our results suggest that circumneutral iron-rich deposits should be deprioritized in favor of acidic iron- and sulfur-rich deposits when searching for evidence of life with solvent extraction techniques. Key Words: Mars—Biosignature—Hydrous pyrolysis—Kinetic parameters—Lipids—Artificial maturation. Astrobiology 21, 638–654.

1. Introduction

The successful search for life on Mars is dependent on the careful consideration of rocks that reflect deposition in environments that are likely to have supported life. Iron-rich, aqueous environments provide habitable niches on Mars due to the availability of dissolved Fe(II) that can drive both aerobic and anaerobic microbial metabolism (*e.g.*, Widdel *et al.*, 1993). Iron is an abundant element in martian regolith and is an especially powerful biogeochemical element due to its ability to act as both an electron donor for iron-oxidizing bacteria (Baker and Banfield, 2003; Emerson and Weiss, 2004), and an electron acceptor in dissimilatory iron reduction processes (Lovley, 1991). Subsurface or subaqueous chemolithotrophs may have existed on early Mars and taken advantage of the abundant iron present on the red planet.

Iron-rich environments have, historically, been considered deleterious to organic matter preservation due to the predisposition of iron to oxidizing reactions (Sumner, 2004; Klein, 2005), but they are becoming increasingly accepted as capable of preserving microbial biosignatures, either in the form of structural biosignatures due to iron oxide encrustation (Potter-McIntyre *et al.*, 2014; Williams et al., 2015a, 2016) or molecular biomarkers in the form of lipids that survive the initial stages of diagenesis by being encrusted or adsorbed onto the surface of amorphous, high-surface-area iron oxides, and oxyhydroxides (Lalonde *et al.*, 2012; Parenteau et al., 2014, 2016; Tan *et al.*, 2018).

Department of Earth Science and Engineering, Impacts and Astromaterials Research Centre, Imperial College London, London, United Kingdom.

© Jonathan S. W. Tan and Mark A. Sephton, 2021; Published by Mary Ann Liebert, Inc. This Open Access article is distributed under the terms of the Creative Commons Attribution Noncommercial License (http://creativecommons.org/licenses/by-nc/4.0/) which permits any noncommercial use, distribution, and reproduction in any medium, provided the original author(s) and the source are credited.

Low-temperature, circumneutral, iron-rich aqueous environments have recently been the subject of significant interest due to observations made by the Mars Science Laboratory (MSL) rover Curiosity that suggest the presence of a circumneutral, low-salinity, possibly redox-stratified iron-rich lacustrine environment that existed between 3.8 and 3.1 Ga at Gale Crater (Hurowitz et al., 2010, 2017; Grotzinger et al., 2014, 2015; McLennan *et al.*, 2014; Vaniman *et al.*, 2014; Bristow *et al.*, 2015). The primary iron species found in similar terrestrial settings is ferrihydrite, a nanocrystalline iron oxide ($Fe_5HO_8 \cdot 4H_2O$) that exists in two forms, ''2-line ferrihydrite'' and ''6-line ferrihydrite,'' that are distinguished by the degree of crystallinity that it exhibits according to the presence of X-ray diffraction (XRD) lines (Cornell and Schwertmann, 2003).

Ferrihydrite comprises a majority of the X-ray amorphous component in the martian regolith, being present in proportions of up to 50 wt% in mudstones examined at Yellowknife Bay (Dehouck *et al.*, 2017). Ferrihydrite is also found in a wide variety of martian environments, such as in the Rocknest, Cumberland, and Windjana samples as analyzed by CheMin on the MSL Curiosity rover (Bish *et al.*, 2013; Vaniman *et al.*, 2014; Rampe *et al.*, 2016; Treiman *et al.*, 2016; Dehouck *et al.*, 2017), at Gusev Crater and Meridiani Planum as observed by the Mars Exploration Rover missions (Morris et al., 2006a, 2006b), and other locations such as McLaughlin Crater as observed by the Compact Reconnaissance Imaging Spectrometer for Mars (Michalski *et al.*, 2019).

Due to the metastability of ferrihydrite, this mineral is often not found in terrestrial sediments and rocks older than the Holocene, and it is instead a precursor to more stable iron oxide species such as goethite (α-FeOOH) and hematite (α-Fe_2O_3) (Cornell and Schwertmann, 2003). On Mars, however, the low-temperature, rock-dominated environment inhibits the transformation of ferrihydrite even when subjected to short-term aqueous alteration (Dehouck *et al.*, 2017). The widespread, long-term preservation of ferrihydrite at Gale Crater over geological time, its ubiquity in the martian surface and subsurface, and the possibility that it may have supported biological activity suggest that ferrihydrite has the potential to be a target of astrobiological interest.

Little is known, however, about the degradation reactions, mechanisms, and organic matter–mineral interactions associated with biomarker preservation in ferrihydrite, especially with respect to the processes and fluxes associated with the post-burial effects of diagenesis. In particular, rapid burial is relevant to biomarker preservation not only as a degradative process but also as a mechanism by which the organic biomarkers contained within these sediments and rocks may be shielded from deleterious radiation, such as solar ultraviolet radiation or galactic cosmic rays (Cockell *et al.*, 2005; Dartnell *et al.*, 2007; Dartnell, 2011; Cockell, 2014; Hassler *et al.*, 2014). Planned missions to Mars such as ExoMars have been designed with the aim of collecting samples that have been shielded from surface radiation, where a drill will be used to access samples at depths of up to 2 m (Vago *et al.*, 2016). Other strategies include targeting surfaces that have only recently been exhumed such as near escarpments or at sites of impact ejection (Farley *et al.*, 2014; Montgomery *et al.*, 2016). It is, therefore, necessary to elucidate the relationship between organic matter, minerals, and their interactions during diagenesis.

Recent geochemical work has focused on using hydrous pyrolysis to expound on the post-burial effects of diagenesis on the degradation of specific organic compounds in Mars-analog geochemical environments (*e.g.*, Royle *et al.*, 2018; Tan *et al.*, 2018; Tan and Sephton, 2020). Hydrous pyrolysis has traditionally been used to study the diagenesis and maturation of organic compounds as it replicates the organic geochemical reactions that occur over geological timescales by simulating them with short-term, high-temperature, and high-pressure laboratory conditions; this technique has been utilized by several authors to study the effects of thermal maturity on specific biomarker compounds (*e.g.*, Eglinton *et al.*, 1986; Peters *et al.*, 1990; Koopmans *et al.*, 1995; Jaeschke *et al.*, 2008; Rush *et al.*, 2014; Royle *et al.*, 2018).

By analyzing the products of artificial maturation experiments under laboratory conditions and deriving the kinetic parameters of organic matter breakdown, it is possible to determine the optimal conditions under which preservation is favored, and this can also help to quantitatively predict the effects of degrading reactions on organic biomarker concentrations over geological time. Here, we present the results of hydrous pyrolysis experiments performed on ferrihydrite deposits found flocculating in a circumneutral, iron-rich bog. We report on the complex interactions between the hosted organic matter and the ferrihydrite-rich mineralogy of the deposits, their response to the post-burial stresses of diagenesis, and the applications of our findings to future missions to Mars.

2. Materials and Methods

2.1. Sample collection

The geology of the Imperial College Silwood Park Campus is located stratigraphically at the base of the Bracklesham Group, a series of Eocene deposits (50–44 Ma) that comprise the Camberley, Windlesham, and Bagshot iron-rich sand horizons that, in turn, overlie the impermeable London Clay (Barrott *et al.*, 2014). The downward permeation of groundwater in these sand horizons has resulted in the anaerobic leaching of Fe(III) from glauconite hosted within these deposits, leading to the widespread occurrence of circumneutral iron seeps rich in dissolved Fe(II) (Barrott *et al.*, 2014). Fe-rich groundwater discharges from sand horizons are rare, as the depletion of reactive iron from ferruginous sands is a geologically rapid process. The Bracklesham Group is unique, as the groundwater in this region was relatively isolated from the surface until the last deglaciation; the iron seepage in this area is, thus, a geologically ephemeral process and is expected to continue only for another 0.1 Ma (Barrott *et al.*, 2014).

This iron-rich groundwater system is manifested as a large iron bog $\sim$20 by 30 km in area, with springs rich in Fe^{2+} emerging from various locations depending on the topography, and it is defined by an ocherous color derived from the precipitation of iron oxides by iron-oxidizing bacteria (FeOB). Streamwater conditions were found to have a temperature of $\sim$10°C, with circumneutral pH and containing 10–20% dissolved oxygen, consistent with its provenance as groundwater flow (Barrott *et al.*, 2014). The sampling area was limited to the lacustrine and stream environment accessible from the Imperial College Silwood Park campus owing to safety concerns (Fig. 1a, b).

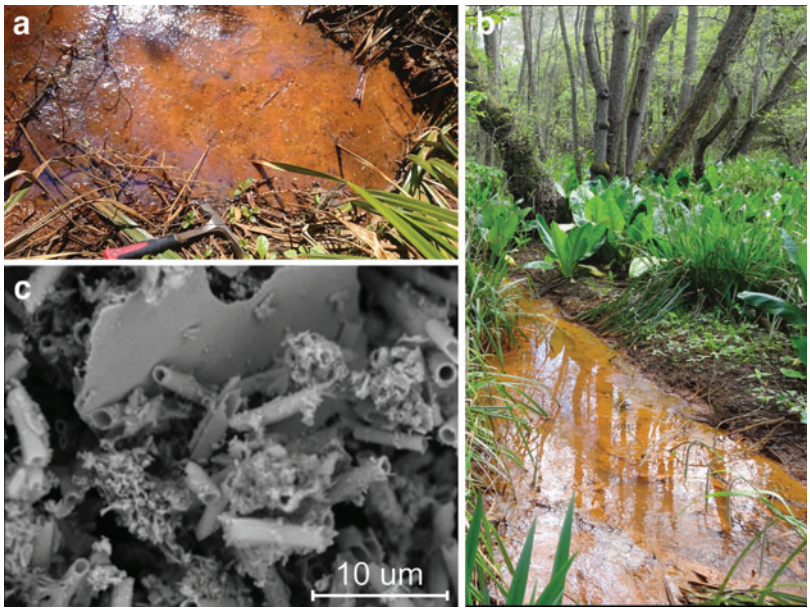

FIG. 1. Field and SEM images of the sampling sites. **(a)** Silwood Site 6. Samples were taken from a small ''bay'' where there is little streamwater flow. A thin microbial film is observed over the surface of the still water. **(b)** Sunninghill Bog. Streamwater flow here is faster than at Silwood Site 6, but iron flocs can still be observed. **(c)** SEM images of the ferrihydrite flocs. Clear structural biosignatures characteristic of *Leptothrix ochracea* are observed, forming hollow, cylindrical sheaths ~1 μm across. All samples imaged featured these biostructures. Photos taken by Jonathan Tan and Mark Sephton (2017). SEM, scanning electron microscopy. Color images are available online.

Ocherous, highly amorphous, ferrihydrite flocs were precipitated in these environments by FeOB via the conversion of dissolved ferrous iron into insoluble ferric iron as part of their metabolic pathways (Chan *et al.*, 2016). These flocs encrusted the bacteria that precipitated them, forming filamentous sheaths that could be clearly observed in scanning electron microscopy (SEM) images (Fig. 1c). These sheaths were identified as characteristic biostructures of *Leptothrix ochracea*, a chemolithoautotrophic FeOB (Emerson *et al.*, 2010; Fleming *et al.*, 2014; Chan *et al.*, 2016). *L. ochracea* is capable of oxidizing Fe at a range of O_2 concentrations, and it flourishes at microaerobic conditions down to 30 μM dissolved O_2 (Chan *et al.*, 2016; Fleming *et al.*, 2018). The filamentous sheaths produced by *L. ochracea* and iron oxidation during metabolism are known to be tightly coupled, indicating a strong association between precipitated ferrihydrite and organic matter in these flocculent mats (Chan *et al.*, 2016; Vesenka *et al.*, 2018).

Samples of flocculent ferrihydrite were collected by filtering streamwater through VWR 12–15 μm filter paper and transferring the ocherous residue to falcon tubes pre-washed in deionised (DI) water. The residues were returned to the laboratory, freeze-dried, and powdered with a solvent-cleaned agate pestle and mortar.

2.2. Scanning electron microscopy

The filamentous sheaths present in the ferrihydrite flocs were imaged with a Phenom ProX Desktop SEM. The samples were loaded onto an SEM sample stage by using a double-sided carbon tape. The SEM was operated at 5 kV with a working distance of 5.9 mm. Images were taken at magnifications of ~10,000, 25,000, 50,000, and 100,000.

2.3. Ferrihydrite synthesis

Synthetic 2-line ferrihydrite was made following the method detailed in Cornell and Schwertmann (2003). Eight grams of $Fe(NO_3) \cdot 9H_2O$ (Sigma-Aldrich, suitable for cell culture) was dissolved in 100 mL of DI water and stirred with a magnetic stirrer. Sixty-six milliliters of 1 M potassium hydroxide (KOH) solution was continuously added, and the pH of the resulting mixture was brought to 7.5. The final volume of KOH solution was added dropwise, and the pH was continuously monitored. Dissolved salts were removed by adding DI water, centrifuging, and decanting the supernatant until the conductivity was <10 μS/cm as measured with a total dissolved solids probe. The synthesized ferrihydrite was then freeze-dried and ground gently in a solvent-cleaned agate pestle and mortar. It was then analyzed by powder XRD to ensure that the products were amorphous and analogous to the mineral content of the natural ferrihydrite (NF) (Fig. 2). As ferrihydrite is known to recrystallize at room temperature, synthetic samples were wrapped in aluminum foil and stored at 4°C.

2.4. Artificial maturation by hydrous pyrolysis

NF samples from Silwood Site 6 (hereafter referred to as NF) and the synthetic ferrihydrite (SF) samples produced under laboratory conditions (hereafter referred to as SF) were chosen for artificial maturation by hydrous pyrolysis. The two samples were selected to distinguish the mineralogical differences associated with iron species transformation in the presence or absence of organic matter (NF and SF, respectively). A list of experimental conditions and sample names is presented in Table 1.

Hydrous pyrolysis experiments were set up as described in previously published artificial maturation studies (Royle *et al.*, 2018; Tan and Sephton, 2020). A high-temperature and high-pressure stainless steel reactor (70 mL Model 4740; Parr Instruments) was used for these experiments. To accommodate the small sample sizes, small stainless steel ''bomblets'' were constructed by using T316 ½-inch stainless steel tube (35 × 9 mm o.d. × 6 mm i.d.) sealed at both ends with Swagelok end caps (SS-600-C) after deburring, with a final internal volume of ~1.5 mL. Before each experiment, the bomblets were ultrasonically washed for 10 min in deionized (DI) water, methanol, and dichloromethane, and they were dried at 110°C.

Each sample was loaded into the bomblet, and either 0.1 or 0.5 mL of degassed DI water was added depending on the

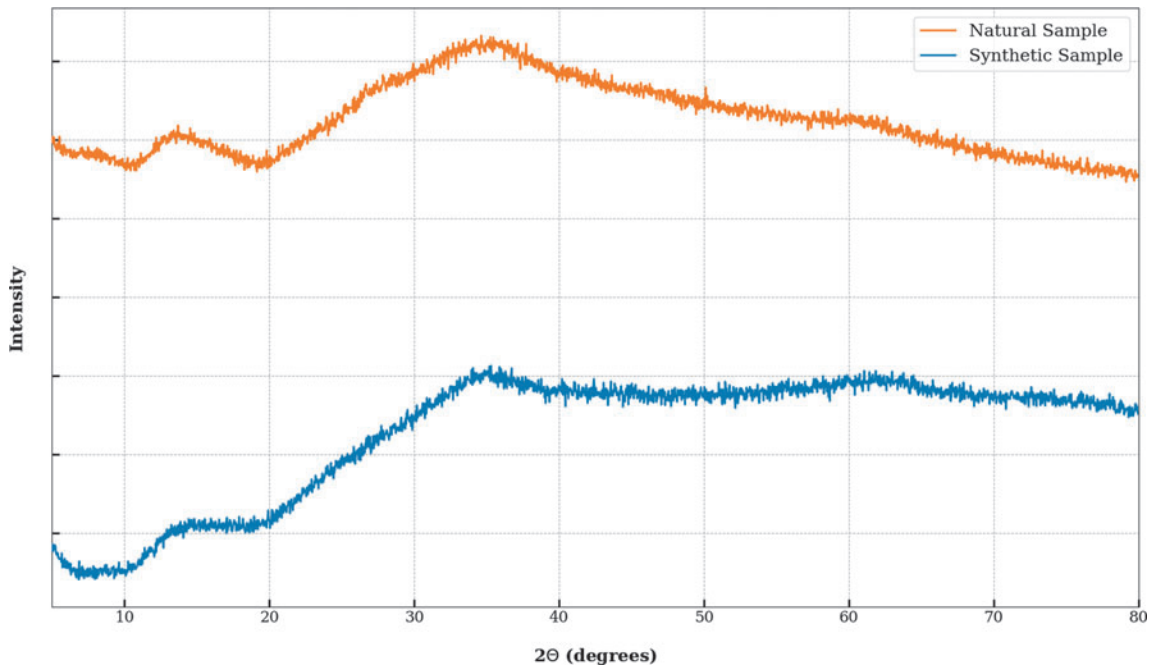

FIG. 2. Comparison between XRD spectra of natural and synthetic ferrihydrite samples. XRD, X-ray diffraction. Color images are available online.

water-to-rock ratios to be studied. The bomblets were sealed in nitrogen gas to mimic an anoxic atmosphere and thoroughly shaken to ensure homogenisation. Up to two bomblets were inserted into the Parr reaction vessel per run. Twenty milliliters of degassed DI water was added to the vessel to ensure a reduced pressure differential across the bomblet walls. The reaction vessel was then heated to the appropriate temperatures in a muffle furnace for 72 h (Table 1). Samples hydrously pyrolyzed at 100°C and below were found to result in changes in lipid abundance that were smaller than the measurement errors associated with the solvent extraction process. Hence, these samples were pyrolyzed for a period of 1 month to ensure observable changes in lipid abundance before and after artificial maturation, a period that has historically been used in previous hydrous pyrolysis studies (Lewan, 1985; Lewan *et al.*, 1986) and that is well beyond the time that changes in lipid abundance would have stabilized (Leif and Simoneit, 1995).

Table 1. List of Samples Subjected to Hydrous Pyrolysis

Mineral type	*Sample code*	*Sample (mg)*	*Water (mL)*	*Temperature (°C)*
Natural ferrihydrite				
	NF-unheated	0.337	N/A	Not heated
	NFL-25-MO	0.0284	0.1	25
	NFL-40-MO	0.0243	0.1	50
	NFL-100-MO	0.0242	0.1	100
	NFL-150	0.0207	0.1	150
	NFL-200	0.0218	0.1	200
	NFL-240	0.0241	0.1	240
	NFL-280	0.0232	0.1	280
	NFH-25-MO	0.0284	0.5	25
	NFH-40-MO	0.023	0.5	50
	NFH-100-MO	0.0306	0.5	100
	NFH-150	0.0206	0.5	150
	NFH-200	0.0343	0.5	200
	NFH-240	0.0330	0.5	240
	NFH-280	0.0334	0.5	280
Synthetic ferrihydrite				
	SF-50	0.0685	0.5	50
	SF-100	0.0903	0.5	100
	SF-150	0.0933	0.5	150
	SF-200	0.0863	0.5	200

Samples with the MO suffix were artificially matured for 1 month, and all other samples were matured for 72 h.
N/A = not applicable; NF = natural ferrihydrite; NFH = natural ferrihydrite pyrolyzed at high water-to-rock ratios; NFL = natural ferrihydrite pyrolyzed at low water-to-rock ratios; SF = synthetic ferrihydrite.

2.5. Pyrolysate extraction

The pyrolysates were extracted from the bomblets by using the method described in the work of Tan and Sephton (2020). A total of 5 μL of a 1.0 mg/mL 5β-cholanic acid and 0.5 mg/mL *p*-terphenyl mixture was added to the sample and used as an internal standard for quantification purposes. The sample was then concentrated in a rotary evaporator and dried by using anhydrous sodium sulfate.

The hydrous pyrolysates were then treated with boron trifluoride in methanol (BF_3-methanol), as described in the work of Tan *et al.* (2018) to break any ester bonds present. This transesterification treatment liberated fatty acids and converted them to fatty acid methyl esters that were more amenable to gas chromatography-mass spectrometry (GC-MS) analysis. The hydrous pyrolysates were then further derivatized with 99-1 *N*,*O*-bis(trimethylsilyl) trifluoroacetamide-trimethylchlorosilane to silylate any remaining hydroxyl groups.

2.6. Gas chromatography-mass spectrometry

GC-MS analyses of the hydrous pyrolysates were conducted with an Agilent Technologies 7890 GC coupled to a 5973 MS. Injection (1 μL) was injected with a split ratio of 10:1, with helium carrier gas at a constant flow rate of 1.1 mL/min. Separation was performed on a J&W DB-5MS UI column (~30 m in length, 0.25 mm internal diameter, and a film thickness of 0.25 μm). The GC oven temperature was held at 40°C for 2 min and then ramped at 5°C/min to 310°C, where it was held for 9 min. Mass spectra were acquired in the scan range (45–550 amu). Peak identification was based on retention time and mass spectra comparisons with authenticated standards and by reference to the NIST-08 mass spectral database.

2.7. Kinetic parameter modeling

The kinetic parameters of the degradation reaction can be derived from the ratio of lipid abundances before and after artificial maturation (Royle *et al.*, 2018). Assuming first-order reaction kinetics, it is possible to derive the activation energy E (J/mol), and the Arrhenius constant A (s^{-1}) from the linear form of the Arrhenius equation (Eq. 1), which relates the aforementioned parameters with the reaction rate constant, k (s^{-1}), the absolute temperature T (K), and the gas constant R (J/mol/K).

$$\ln k = -\frac{E_a}{R}\left(\frac{1}{T}\right) + \ln A \quad (1)$$

The derived kinetic parameters of these organic degradation reactions include any additional effects promoted by the intersections between the organic matter and the mineral matrix. The preservation of organic biomarkers in these specific environments can then be modeled over geological time (Lewan, 1985; Hunt *et al.*, 1991), and it can be specifically adjusted for martian geological time for any given Mars-relevant temperature profile (Royle *et al.*, 2018).

2.8. X-ray diffraction

The mineralogy of both the NF and SF samples was characterized by XRD before and after pyrolysis. Samples were mounted in a flat holder, and powder XRD patterns were acquired by using a PANalytical X'Pert Pro MPD Alpha-1 X-Ray Diffractometer with an X'Celerator detector. Samples were analyzed between 5° and 80° 2θ under copper radiation with a step size of 0.033° at a speed of 5° per minute. Measurements were made at a current of 40 mA and a voltage of 40 kV. The diffraction patterns were analyzed with an X'Pert Highscore Plus program with references from the International Centre for Diffraction Data (ICDD) database.

3. Results

3.1. Lipid abundances

Figure 3a and b reveal that the solvent extracts of the unmatured ferrihydrite were found to be composed primarily of fatty acids, including saturated, unsaturated, and terminally branched species, consistent with their high abundance in bacterial cell membrane phospholipids (*e.g.*, Harwood and Russel, 1984; Ratledge and Wilkinson, 1988; Killops and Killops, 2005). The saturated fatty acids were also observed to exhibit a clear even-over-odd predominance (EOP) pattern, which can be used to distinguish the observed lipid profile from non-biological organic matter. The suite of lipids found in these samples is consistent with the results of previous studies focused on lipid preservation in Mars-analog environments (*e.g.*, Parenteau *et al.*, 2014; Wilhelm *et al.*, 2017; Tan *et al.*, 2018).

Figure 3c and d indicate that the unheated NF sample (NF-Unheated) contains ω-hydroxy fatty acids. These molecules are key components of cutin (Kolattukudy and Walton, 1972; Soliday and Kolattukudy, 1977), and thus they are characteristic of higher order plant material. Cutin is formed from the inter-esterification of ω-hydroxy fatty acids; these esters bonds would have been cleaved during the derivatization process. Polycyclic terpenoids such as campesterol, stigmasterol, β-sitosterol, oleanone, and lupenone are also found in the ferrihydrite samples (Fig. 3c, d), and they are also characteristic of higher order plant material. Plants are unlikely to have evolved on Mars, but the observation of how these compounds are affected by simulated diagenesis can shed light on the evolution of other Mars-relevant polycyclic terpenes such as bacterial hopanoids during diagenesis in Mars-like conditions.

All the major lipid groups found in the solvent extracts of each sample were observed to respond strongly to changes in hydrous pyrolysis temperature (Fig. 3a, b). In general, solvent-extractable lipid abundances were found to increase with increasing hydrous pyrolysis temperatures until a peak abundance was reached at around 150°C, after which lipid abundance decreased rapidly with increasing hydrous pyrolysis temperatures. Individual lipid groups followed a similar pattern, with all major groups peaking in abundance between 100°C and 150°C. The exception to this was the polycyclic terpenoids observed in the lower water-to-rock ratio sample, which peaked in abundance at 50°C.

Changes in lipid abundance were investigated between 200°C and 280°C, as these are the temperatures at which the processes of diagenesis are most relevant (Eglinton and Douglas, 1988; Peters *et al.*, 1990; Koopmans *et al.*, 1995; Jaeschke *et al.*, 2008). It was observed that almost all lipid species are destroyed in the presence of ferrihydrite during late-stage diagenesis (hydrous pyrolysis run at 280°C) regardless of lipid group or water-to-rock ratios (Fig. 3c, d).

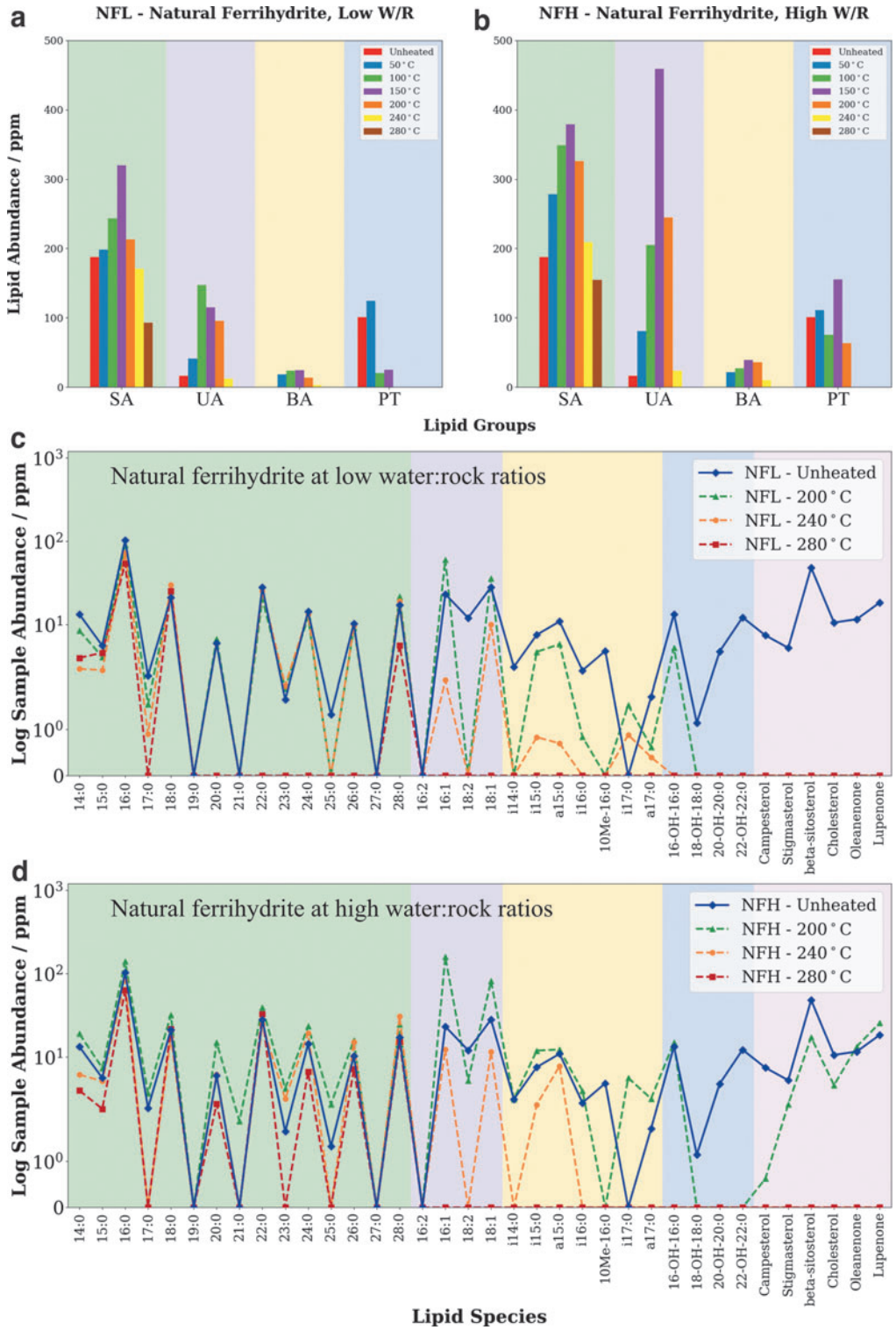

FIG. 3. The variation of the lipid abundance per group of lipids for **(a)** NFL and **(b)** NFH over a temperature range from 50°C to 280°C. In most cases, observed lipid abundance increases with temperature and peaks at 150°C, after which it drops sharply. Lipid abundances in hydrously pyrolysed samples of **(c)** NFL and **(d)** NFL are also presented. The *n*:*m* notation refers to fatty acids with an *n* number of carbon atoms and an *m* number of unsaturated double bonds. The solid line represents total lipid extracts of the unheated natural ferrihydrite sample, whereas the dotted lines indicate the lipid abundances in the hydrous pyrolysates. SA, saturated fatty acids; UA, unsaturated fatty acids; BA, branched fatty acids; PT, polycyclic terpenoids; NFL, natural ferrihydrite pyrolyzed at low water-to-rock ratios; NFH, natural ferrihydrite pyrolyzed at high water-to-rock ratios. Color images are available online.

Saturated fatty acids were observed to be the most resistant of all the major lipid groups. Saturated fatty acids that were retained also preserved their biogenic signatures in the form of an EOP pattern in carbon-chain lengths, consistent with previous hydrous pyrolysis studies of other Mars-analog samples (Tan and Sephton, 2020). In the 280°C hydrous pyrolysis run, only lipids remaining in the NF samples (natural ferrihydrite pyrolyzed at low water-to-rock ratios [NFL] and natural ferrihydrite pyrolyzed at high water-to-rock ratios [NFH]) were saturated fatty acids; 16:0, 18:0, and 28:0 were present in both samples, whereas 20:0, 22:0, 24:0, and 26:0 were present only in NFH. The lack of any of the other lipid groups at lower hydrous pyrolysis temperatures, and even some species of saturated fatty acids, highlights the deleterious effect of ferrihydrite.

Qualitatively, the preservation of lipids appeared to be slightly more favorable in water-dominated environments when pyrolyzed to temperatures between 200°C and 280°C (Fig. 4). This was most clearly seen in the unsaturated fatty acid fraction at 200°C, and the saturated fatty acid fraction at 280°C, where the high water-to-rock ratio samples (NFH) were found to have higher lipid abundances than the corresponding low water-to-rock ratio samples (NFL), and in some cases entire species of fatty acids were preserved compared with rock-dominated environments. The preservation bias of water-dominated environments lessened at higher pyrolysis temperatures, as all lipids were lost regardless of the degree of water activity.

3.2. Mineral transformation in the presence and absence of organic matter

It is well known that iron oxides undergo complex mineral transformations when exposed to increased temperatures and/or in the presence of organic matter (*e.g.*, Cornell and Schwertmann, 2003). To investigate these changes, all samples were visually inspected for differences after each hydrous pyrolysis experiment. The XRD was also conducted on all samples.

The NF samples initially exhibited the characteristic ochre hue as observed at the sampling site at Silwood Park. After hydrous pyrolysis at temperatures ≤100°C, the color of the samples remained unchanged. At temperatures of 150°C or greater, the samples were observed to be pitch black on extraction from the bomblets, suggesting that a change in mineralogy had occurred between the temperatures of 100°C and 150°C.

The XRD analyses of the natural samples at both high and low water-to-rock ratios are shown in Fig. 5. The NF exposed to temperatures of 100°C or lower showed no observable changes compared with the initial samples, and it retained the two broad diffraction peaks that are indicative of poorly crystalline 2-line ferrihydrite (Cornell and Schwertmann, 2003). Diffraction peaks located at 30.14°, 35.50°, 43.15°, 53.54°, 57.04°, and 62.63° 2θ first appeared at 150°C, and they remained present up to 280°C. These peaks were identified as magnetite (Fe_3O_4), the appearance of which corresponded with the color change observed in the physical samples after extraction. Additional magnetite peaks at 18.30°, 37.11°, and 74.17° 2θ were observed in samples pyrolyzed to temperatures of 200°C and above.

The formation of well-defined peaks and the complementary disappearance of the two broad ferrihydrite diffraction peaks suggested that the ferrihydrite was transformed into crystalline magnetite. The appearance of additional magnetite peaks, as well as the sharpening and increasing intensity of pre-existing peaks, suggested that although magnetite transition commenced before 150°C, peak crystallinity was not achieved until 200°C, indicating a transitional temperature range between 100°C and 200°C. No further changes in

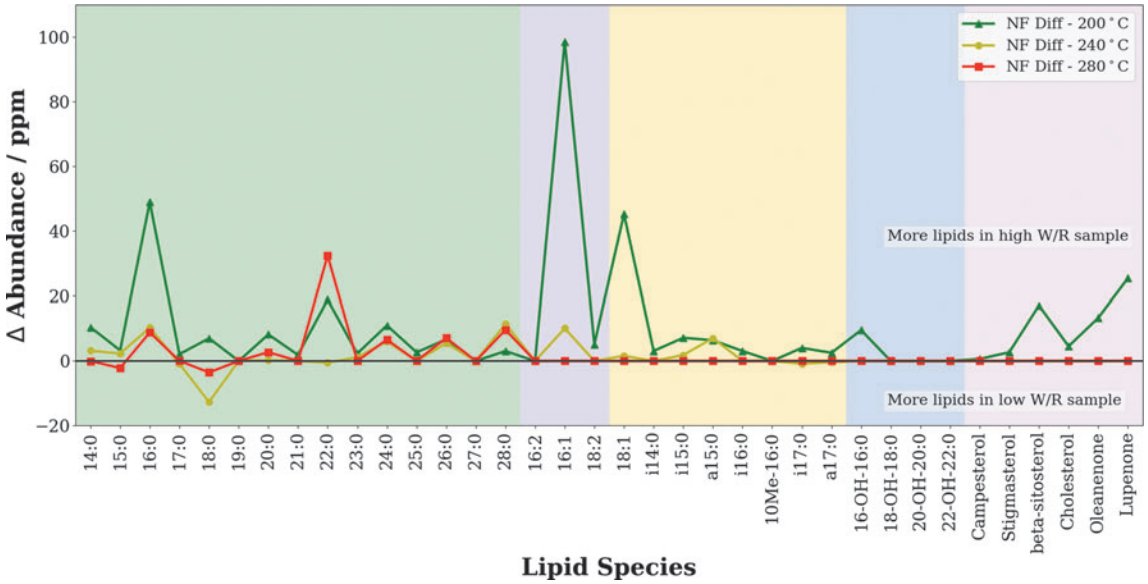

FIG. 4. Graph showing the differences in abundance between individual lipid species in the lipid extracts when comparing the NFH and NFL across hydrous pyrolysis temperatures between 200°C and 280°C. A positive value indicates that more lipids of that species were present in NFH, whereas a negative value indicates that more lipids were present in NFL. Preservation appears to be slightly favored in circumneutral iron-rich environments with higher water availability. Note that most lipid species are lost by 280°C, and hence the difference between the two samples appears to be zero. Color images are available online.

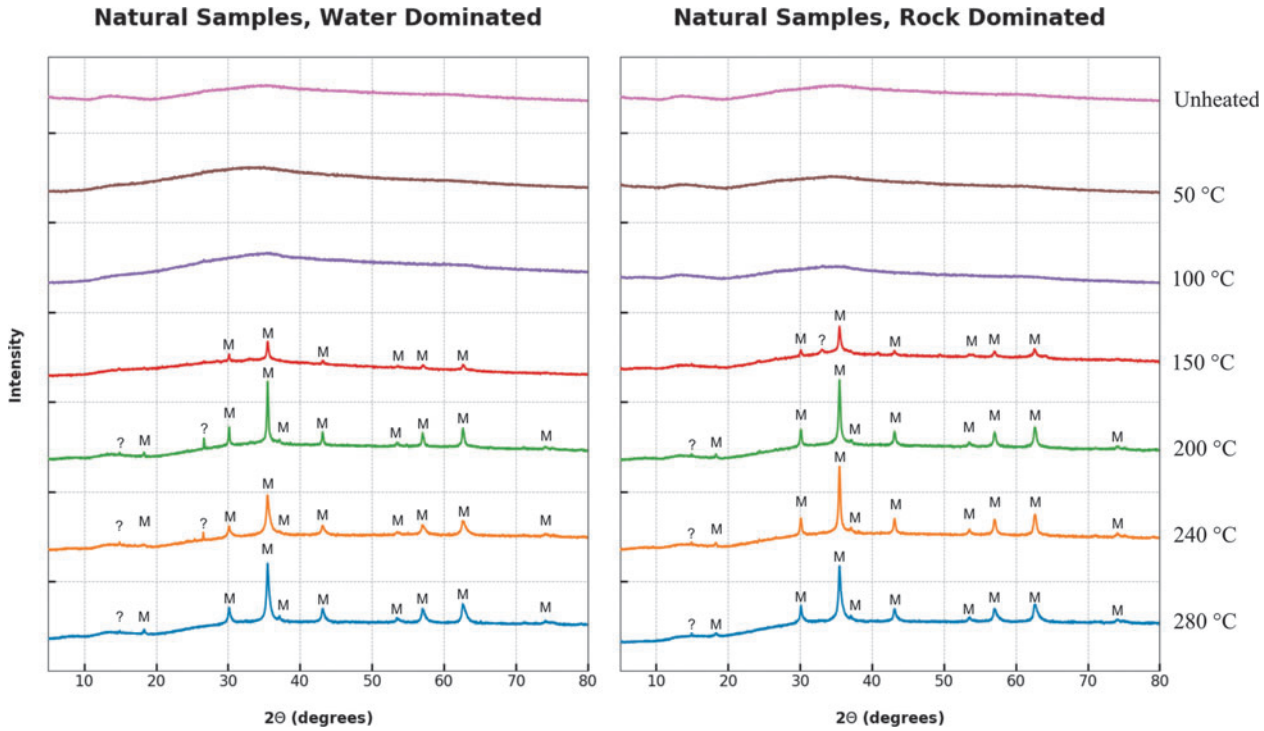

FIG. 5. XRD spectra of unheated and pyrolyzed natural ferrihydrite samples under both rock- and water-dominated conditions. The data clearly show the transformation of ferrihydrite to magnetite (M) at 150°C regardless of water availability. Color images are available online.

mineralogy were observed at temperatures >200°C. Some unidentified peaks were present, but they did not correspond to other iron oxide or oxyhydroxide species.

A similar mineralogical change was observed in the SF samples, although this transformation occurred at a lower temperature. These dark brown precipitates were unchanged until hydrously pyrolyzed at 100°C, on which the samples were observed to have a bright orange coloration on extraction from the bomblets.

No magnetite was observed in the XRD spectra of the SF samples (Fig. 6). Instead, hematite (Fe_2O_3) diffraction peaks were observed at temperatures of 100°C and above, consistent

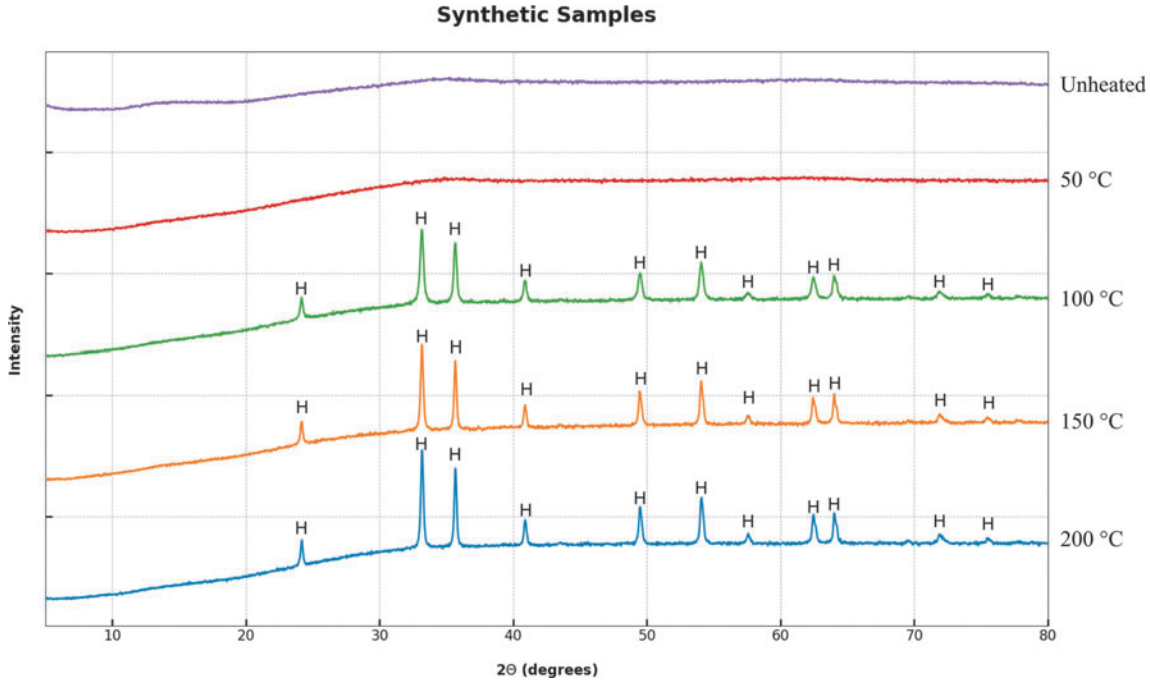

FIG. 6. XRD spectra of unheated and pyrolyzed synthetic ferrihydrite samples. The data clearly show the transformation of ferrihydrite to crystalline hematite (H) at 100°C. Color images are available online.

Table 2. Data Used to Calculate the Kinetic Parameters Associated with Saturated Fatty Acid Degradation Under Varying Mineralogical and Water-To-Rock Conditions

Sample code	C_0/C_t	k (h^{-1})	T (*K*)	*ln* k (h^{-1})	*1*/T (K^{-1})	*ln* k *error*
Natural ferrihydrite, low water-to-rock ratios						
NFL-40-1MO	1.068844	8.95E-05	313	−9.321	0.003195	±0.958
NFL-100-1MO	1.247629	2.97E-04	373	−8.121	0.002681	±0.887
NFL-150	1.248682	3.08E-03	423	−5.781	0.002364	±0.594
NFL-200	1.639856	6.87E-03	473	−4.981	0.002114	±0.544
NFL-240	2.015109	9.73E-03	513	−4.632	0.001949	±0.502
NFL-280	4.282019	2.02E-02	553	−3.902	0.001808	±0.424
Natural ferrihydrite, high water-to-rock ratios						
NFH-40-1MO	1.055211	7.22E-05	313	−9.536	0.003195	±0.990
NFH-100-1MO	1.386775	4.39E-04	373	−7.730	0.002681	±0.818
NFH-150	1.150419	1.95E-03	423	−6.242	0.002364	±0.648
NFH-200	1.30433	3.69E-03	473	−5.602	0.002114	±0.592
NFH-240	1.778214	7.99E-03	513	−4.829	0.001949	±0.512
NFH-280	2.579927	1.32E-02	553	−4.330	0.001808	±0.458

C_0/C_t refers to the ratio of initial and final concentrations of saturated fatty acids; k refers to the rate constant as calculated from C_0/C_t assuming first-order reaction kinetics [$k = \ln(C_0/C_t)/t$, where t is the time of the experiment in hours]. Errors in ln k are from instrument uncertainty.

with the color change observed in the hand specimen. Hematite was identified by clear diffraction peaks at 24.20°, 33.19°, 35.69°, 40.91°, 49.50°, 54.09°, 57.62°, 62.46°, 64.04°, 71.90°, and 75.49° 2θ. As with the natural samples, the loss of the broad diffraction peaks suggested that the ferrihydrite had been fully transformed into crystalline hematite—notably, this transformation had a lower transition temperature than the ferrihydrite–magnetite transition observed in natural samples. No goethite peaks were observed in either natural or synthetic samples. This suggested that organic matter not only provided a reducing environment in which magnetite transformation was favored, but it also inhibited the formation of hematite.

3.3. Survivability of saturated fatty acids as predicted by kinetic modeling

Kinetic parameters related to lipid degradation were derived from the hydrous pyrolysis results. Specifically, the ratio of saturated fatty acid abundance before and after hydrous pyrolysis was chosen for analysis, as these lipids were observed to be the most resilient to degradation (Table 2). It was found that the lipid degradation reaction was well described with a pseudo-first-order approximation. Using the linear form of the Arrhenius equation, we derived the activation energy (E_a) and the Arrhenius constant (also called the frequency factor) (A) for the NF under both high and low water activities (Fig. 7).

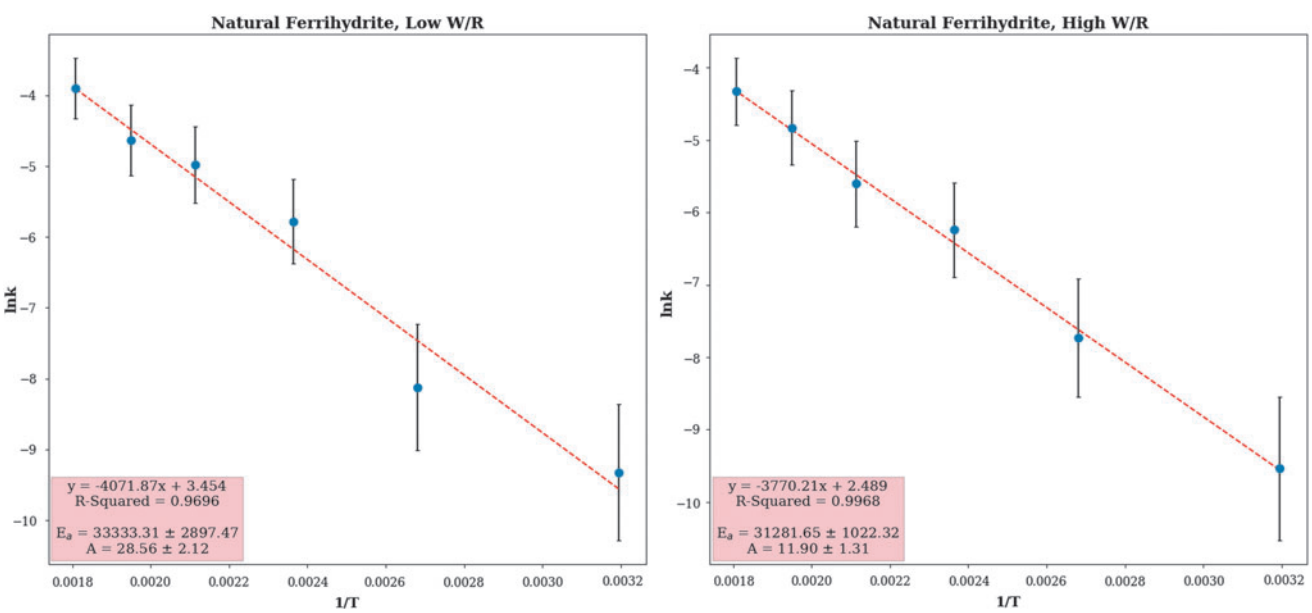

FIG. 7. Kinetic parameters as determined by the linear form of the Arrhenius equation. All data points are well described with a linear trend with high confidence ($R^2 > 0.95$), suggesting that the pseudo-first-order approximation is valid for the lipid degradation reaction. k, rate constant; T, temperature. Color images are available online.

These kinetic parameters were used to model the loss of saturated fatty acids over geological time under Mars-relevant conditions (Royle *et al.*, 2018; Tan and Sephton, 2020). The major assumptions of the model were constant geothermal gradients, surface temperatures, burial and exhumation rates, and a closed system. A temperature profile that represented the best-case scenario for the preservation of organic material was constructed and comprised a geothermal gradient of 0.008 K/m (present day geothermal gradient; Hoffman, 2001), a surface temperature of −50°C (present day average annual equatorial temperature), a burial rate of 10 m/Ma (average burial rates at Gale Crater; Borlina *et al.*, 2015), and a maximum burial depth of 2 m. A more detailed description of how these values were chosen is found in the work of Royle *et al.* (2018).

The model data that represent saturated fatty acid degradation under ferrihydrite-rich Mars conditions are presented in Fig. 8, where t_{max} is the time taken for all saturated fatty acids to be destroyed under the stated temperature and pressure constraints. A full description of how the model was constructed from kinetic parameter data is found in the work of Royle *et al.* (2018). In addition, the link to the freely accessible modeling code is available in the Supplementary Information. The results suggest that all saturated fatty acids would be destroyed within 1 ka under Mars-relevant conditions. Errors in the degradation profile were calculated with the non-linear least-squares method and plotted to show the uncertainties in degradation time, and they are presented as shaded areas in Fig. 8.

4. Discussion

4.1. Organic matter–mineral relationships

Our results suggest that changes in the mineralogy of the iron substrates strongly affect the organic matter–mineral interactions at the surface of the substrate. This is most clearly seen when visualizing the variation in free lipid abundance as the mineralogy of the iron substrate changes (Fig. 9). Between 25°C and 100°C, the ferrihydrite remains amorphous and undergoes no mineralogical changes, whereas the free lipid extract is observed to increase for all lipid groups except for polycyclic terpenoids, which are the most structurally complex and thus most susceptible to degradation. A possible explanation for this phenomenon is the breaking of adsorptive bonds between the sorbed fatty acids and the ferrihydrite substrate via hydrolysis as pyrolysis temperatures increase. This mechanism is likely primarily driven by temperature, hence the increasing abundance of solvent extractable organic matter as temperatures increase. This behavior was also reported in Tan and Sephton (2020), where increased abundances of lipids were observed post-maturation.

At 150°C, the ferrihydrite transforms into magnetite but it does not reach peak crystallinity (Fig. 5). This mineralogical change is accompanied by a sharp increase in the abundance of several lipid groups, including saturated and unsaturated fatty acids (Fig. 9). The release of sorbed materials from ferrihydrite as it undergoes phase transformations has been observed in other compounds such as arsenic (Pedersen *et al.*, 2006), primarily as a result of the surface area of the ferrihydrite becoming too small to retain all the sorbed material (Schikorr, 1933; Booy and Swaddle, 1978; Cornell and Schwertmann, 2003). Organic material entombed within the iron precipitates represents another potential source of solvent-soluble organic matter. Phase transitions in the iron precipitates would likely have released any occluded organic material, rendering them susceptible to solvent extraction. These results suggest that lipids are not necessarily destroyed by the ferrihydrite–magnetite transition and may instead be merely desorbed.

At temperatures between 200°C and 280°C, the magnetite becomes fully crystalline and the abundance of all lipid groups decreases with increasing temperature until all lipids are lost except for the saturated fatty acids. The clear redox effect as

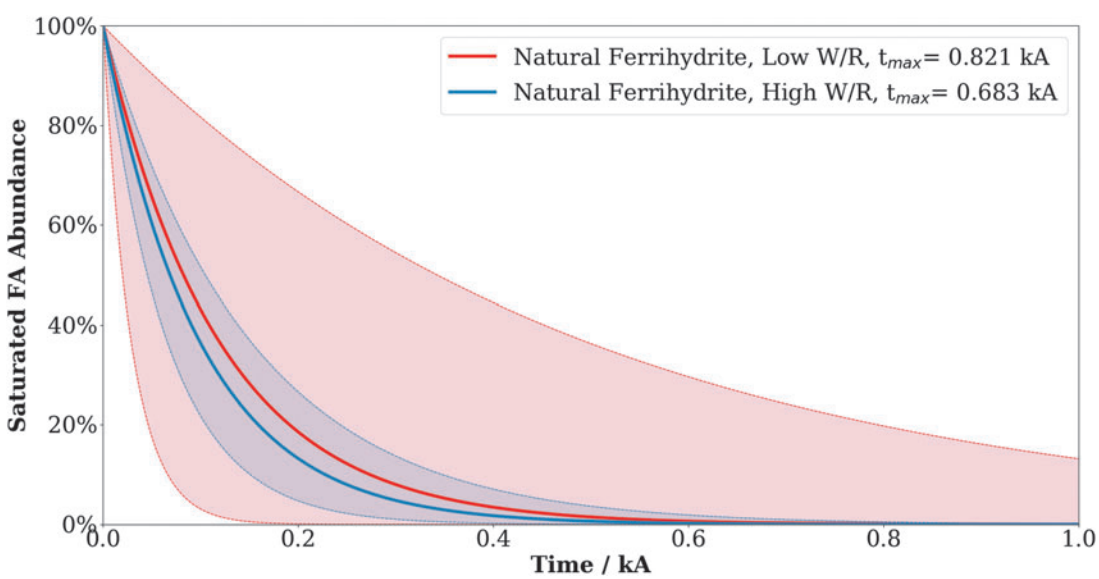

FIG. 8. Model data showing the degradation of saturated fatty acids over geological time under martian surface conditions, with projections derived from the calculated activation energy and Arrhenius constant. Red and blue shaded areas show the uncertainty associated with the timing of degradation of organic matter under low and high water availabilities, respectively. t_{max} values indicate the time at which all fatty acids are lost. At optimal conditions, all saturated fatty acids are modeled to be destroyed within 1 ka, and water availability has no significant effect on degradation rate. Color images are available online.

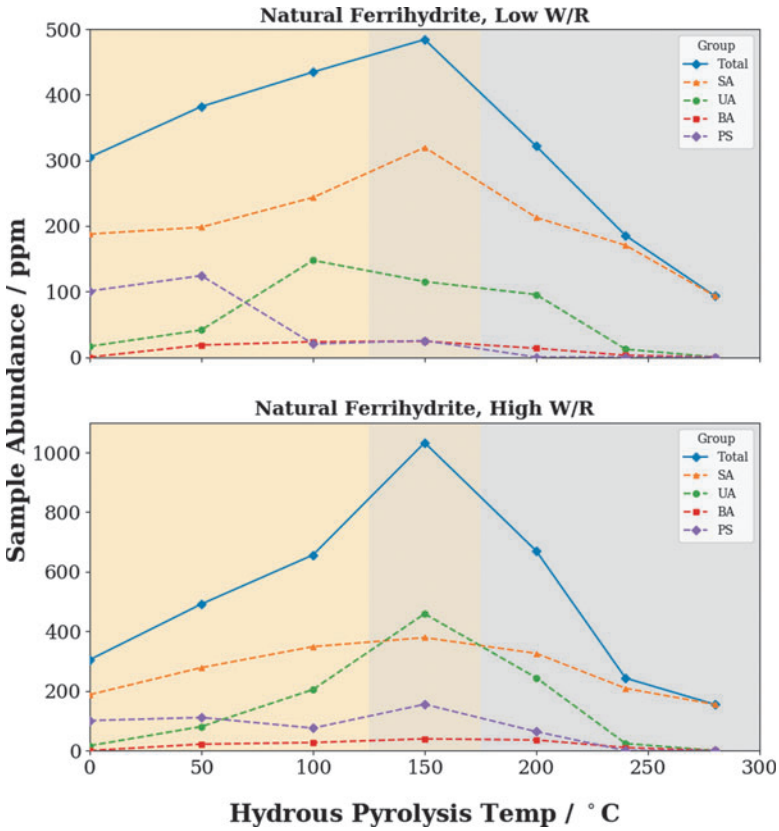

FIG. 9. The variation of abundance of the free lipid extract with increasing pyrolysis temperature. The different-colored backgrounds indicate the mineralogy of the iron oxides; orange indicates ferrihydrite, whereas gray indicates magnetite. Recall that at 150°C magnetite had formed but not yet achieved full crystallinity and is colored slightly darker to reflect this. Color images are available online.

ferric iron in ferrihydrite is transformed to ferrous iron in magnetite, complementary with the loss of organic matter as it is lost due to oxidation, suggests that the primary mechanism by which organic degradation occurs is an oxidative reaction. This is further supported by the lack of alkanes in both the unheated samples and the post-hydrous pyrolysis solvent extracts, suggesting that either decarboxylation is not a significant process during degradation, or that all alkane products were subsequently oxidized, or both.

Our data also suggest that, among the lipid groups, saturated fatty acids are the best targets for life detection missions, as they are the most resistant to degradation and can retain their biogenic EOP signatures, an important quality of potential biosignatures that help distinguish them from abiotic carbon. The suitability of saturated fatty acids as a lipid biosignature is a finding that is consistent with other studies (Tan *et al.*, 2018).

4.2. Iron mineral phase transformations in the presence of organic matter

The presence or absence of organic matter results in significant mineralogical differences when ferrihydrite is heated at anoxic conditions and low water availabilities. In the absence of organic matter, hematite is the dominant iron oxide species, consistent with the results of ferrihydrite evolution at high temperatures as investigated by other authors (*e.g.*, Cornell and Schwertmann, 2003; Dehouck *et al.*, 2017).

In contrast, the natural samples containing a high concentration of organic matter were transformed from amorphous ferrihydrite to crystalline magnetite. Unlike most other iron oxide species, magnetite contains both divalent and trivalent iron cations. For this phase transformation to occur, organic matter must act as the reductant and be oxidized, resulting in the complementary partial reduction of ferrihydrite to magnetite (Booy and Swaddle, 1978; Blesa and Matijević, 1989). These results are consistent with previous work on the heating of ferrihydrite in the presence of organic matter, with magnetite being the sole iron oxide formed as long as excess reductant was present; in samples with insufficient reductant, ferrihydrite was initially reduced to magnetite, and subsequently the ferrous iron present in magnetite was fully oxidized to hematite or maghemite (Campbell *et al.*, 1997; Bishop et al., 2006, 2008).

The lack of hematite or maghemite in the post-maturation NF samples indicates that the OM:Fe ratio was greater than the threshold at which magnetite transforms into either of those iron oxide phases. On Mars, where the biomass of any microbial community may have been limited, the final iron phase may instead be maghemite—the natural oxidation product of magnetite, sharing its structural form while possessing only Fe(III) ions (Fasiska, 1967; Cornell and Schwertmann, 2003; Bishop *et al.*, 2008).

In addition to the reducing effect of organic matter, the results suggest that the presence of organic matter also inhibits the transformation of ferrihydrite into hematite. In the absence of organic matter, SF is transformed into hematite at 100°C. In the presence of organic matter, however, ferrihydrite remains stable past 100°C, and instead it is only transformed into magnetite at 150°C.

The inhibitory effect of organic acids on ferrihydrite crystallization has been noted earlier: Ferrihydrite formation in soils is stabilized by the presence of organic matter, and both the concentration and type of organic acids have been

shown to have a strong effect on ferrihydrite crystallization (Schwertmann, 1966). Carboxylic acids reduce the rate of crystallization of the iron oxide products as well as inhibit the formation of goethite in favor of hematite, whereas hydroxy fatty acids completely inhibit the crystallization of ferrihydrite (Schwertmann, 1970; Cornell, 1979; Kandori *et al.*, 1992). It has been suggested that the adsorption of organic acids onto the surface of the amorphous ferrihydrite prevents crystallization from occurring through the formation of organic ''bridges'' that link multiple ferrihydrite particles (Cornell, 1979).

On Mars, it is unlikely that ferrihydrite deposits would be transformed into other iron oxides by purely diagenetic processes in low-temperature conditions. The presence of stable ferrihydrite dating back to the deposition of the Sheepbed mudstone suggests that ferrihydrite is stable on the surface of Mars and does not oxidize to hematite or magnetite even under the highly oxidizing martian surface conditions (Vaniman *et al.*, 2014; Treiman *et al.*, 2016; Dehouck *et al.*, 2017). A potential conclusion is that outcrops containing extensive hematite derived from ferrihydrite precursors may not be good targets for astrobiological missions, as this would indicate a lack of organic material that would have prevented hematite recrystallization.

4.3. Implications of kinetic modeling

The nature of organic degradation in the subsurface of these ferrihydrite-rich environments was investigated by kinetic modeling. Our data show that the preservation potential of solvent-extractable organic matter in these iron-rich sediments is extremely poor, with all saturated fatty acids lost within 1–3 ka, even under optimal conditions. Current understanding of the hydrological and geological history of Mars suggests that the latest period during which the martian surface was habitable was 3 Ga ago, during the Noachian and Hesperian (Cockell, 2014; Westall *et al.*, 2015). The results of the kinetic modeling, thus, indicate that any ancient circumneutral iron-rich environments would not be able to preserve any deposited solvent-extractable molecular biosignatures to the present day.

The model also suggests that in iron-dominated environments, the kinetics of the oxidation reaction is purely thermally driven. Figure 7 shows that the same kinetic parameters can be applied at all temperatures, regardless of mineralogical transformations, iron mineralogy, and water availability. This was surprising, as current understanding would suggest that iron mineralogy and transformations should have an effect on degradation rate, as the amorphous ferrihydrite would confer the protective qualities associated with the formation of absorptive bonds and organo-metallic complexes (*e.g.*, Lalonde *et al.*, 2012). These protective qualities would eventually be lost at higher temperatures, as lipids are released from the surface of the ferrihydrite by thermal agitation, as well as by the restructuring of ferrihydrite as it is transformed into magnetite. Similarly, water availability should influence lipid degradation, as low water-to-rock ratios have been shown to heighten both protective and degradative effects of the mineral matrix in pyrolysis experiments (Tannenbaum and Kaplan, 1985; Koopmans *et al.*, 1998).

Instead, our results suggest that the breaking of adsorptive bonds between the fatty acids and the iron surfaces via thermal agitation and/or the release of lipids during mineralogical transformations does not necessarily make the lipids more kinetically susceptible to oxidation. They also suggest that neither changes in oxidation state and surface chemistry between ferrihydrite and magnetite, nor differing water availabilities significantly contribute to the overall loss of organic matter in these samples (Fig. 8). Although this cannot be extrapolated to all iron oxide species, our results imply that the rate of degradation in environments dominated by iron oxides/oxyhydroxides is primarily a function of temperature rather than of organic matter–iron mineral interactions and/or water availabilities.

As with all models that attempt to simplify and predict the complexities of the natural environment, it is important to understand the full extent of assumptions made in the construction of this model (an exhaustive list is presented in Tan and Sephton, 2020). In brief, the model assumes a closed system environment, and thus does not account for any open system processes such as the influence of hydrothermal and diagenetic fluids, which are likely to have existed during early Mars (Duda *et al.*, 2018). In the case of hydrothermal systems, other preservative mechanisms associated with the hydrothermal environment, such as permineralization, may allow for better survivability of biosignatures than would be expected from this study (*e.g.*, Cady and Farmer, 1996; Farmer and Des Marais, 1999; Phoenix *et al.*, 2000; Konhauser *et al.*, 2001; Ferris and Magalhaes, 2008).

The model also makes no attempt to determine whether any surviving organic matter can be distinguished from abiotic sources of carbon such as meteoritic material, or organic matter produced from Fischer-Tropsch-type reactions; these materials and processes can produce saturated fatty acids (Chyba and Sagan, 1992; McCollom and Seewald, 2006; Summons *et al.*, 2008; Sephton, 2012; Mißbach *et al.*, 2018).

It is important to emphasize that this simulation only accounts for lipids that are extractable when using wet chemistry, that is, soluble organic matter, and does not preclude the survival of insoluble macromolecular organic matter such as kerogens, which have been shown to be present on Mars (Eigenbrode *et al.*, 2018). Other studies (*e.g.*, Watson and Sephton, 2015) have shown that iron oxides can aid the preservation of organic matter in the form of macromolecular material via catalytic oxidative polymerization. Recent experiments have also shown that macromolecular organic matter can survive artificial maturation and be detected by using thermal extraction techniques such as pyrolysis-gas chromatography-mass spectrometry (Tan *et al.*, 2020). If preparative chemistry steps, such as alkali/acid leaching, are taken before analysis, the macromolecular organic matter detected by flash pyrolysis can also reveal diagnostic biogenic information (Tan *et al.*, 2020).

Regardless of the process by which the saturated fatty acids were lost, the current study suggests that evidence of extinct life would not be preserved in a solvent-extractable form and advocates that purely iron-dominated environments should not be the targets of life detection methods that are reliant on solvent extraction techniques.

4.4. Quantitative comparisons to other Mars-analog environments

One of the primary benefits of kinetic modeling derived from hydrous pyrolysis experiments is that it provides an

experimental standard by which the preservation potential of different Mars-analog environments can be quantified. This allows for a ranking of Mars-analog deposits in terms of which environment is the most likely to preserve any detectable evidence of organic matter.

We compared the preservation potential of iron-rich circumneutral deposits with iron-rich acid deposits by using previous work that utilized the same hydrous pyrolysis/kinetic modeling experiments (Table 3) (Tan and Sephton, 2020).

In Table 3, the preservation potential factor of each Mars-analog environment was based on the expected time it takes for all saturated fatty acids to be destroyed under best-case scenario martian surface conditions by normalizing the values to 1 ka. This allows us to gain quantitative insights into the relative preservation potential of various Mars-analog environments.

Under these parameters, the results suggest that the preservation potential of circumneutral iron-rich deposits is similar to that of iron-rich acid deposits that contain a minor clay component. However, it can be clearly seen that it is much more desirable to target acidic iron-rich deposits that do not contain a clay component for sample selection, as solvent-extractable organic matter is expected to survive between 20 and 100 times longer in those sediments compared with the other Mars analogues that have been studied.

These quantitative results are consistent with previous work, which has shown that clay content catalyzes the breakdown of solvent-soluble organic matter (Tan and Sephton, 2020 and references therein). In addition, circumneutral pH favors the precipitation of amorphous ferrihydrite compared with the more crystalline goethite or hematite that is favored in acidic conditions (Dehouck *et al.*, 2017). The increased surface area of ferrihydrite compared with goethite or hematite leads to a more deleterious environment, resulting in a lower preservation potential.

4.5. Applications to Mars

This study has shown that sediments where ferrihydrite or magnetite are the only mineral phase, or where these iron oxides dominate the mineralogy, are poor targets for wet chemistry GC-MS experiments. Both ferrihydrite- and magnetite-rich sediments are found to be deleterious to organic matter due to the oxidizing power of ferric iron within their structures and they have the same oxidative effect on organic material regardless of provenance, organic matter–mineral interactions, and water availability.

Although our work highlights the poor long-term preservation potential for organic matter in iron-rich environments, it should be noted that iron oxides on Mars are not as widespread as previously believed; the mineralogical data collected by the Chemistry and Mineralogy (CheMin) instrument on the MSL Curiosity rover show that hematite abundance is lacking in a majority of the analyzed mudstone samples (*e.g.*, Bish *et al.*, 2013; Vaniman *et al.*, 2014; Treiman *et al.*, 2016; Rampe *et al.*, 2017; Morris *et al.*, 2019). However, even within the subset of iron-dominated environments on Mars, our results suggest that circumneutral iron-rich deposits should be deprioritized in favor of iron- and sulfur-rich acid deposits when searching for evidence of life with solvent extraction techniques.

The organic matter–mineral interactions revealed by this study can shed light on processes that may be occurring on the present-day surface of Mars, specifically in environments where iron phases contribute to, but do not dominate, the overall mineralogy of the rock. As indicated by the low-temperature maturation experiments, lipids are adsorbed to the surfaces of amorphous iron phases and are only liberated at higher temperatures. In environments such as those observed in Gale Crater, where ferrihydrite has been shown to be a stable, amorphous iron phase but does not dominate the mineralogy of the analyzed mudstones (Vaniman *et al.*, 2014; Treiman *et al.*, 2016; Dehouck *et al.*, 2017), fossil lipids may still remain adsorbed to the amorphous iron phase, especially as organic matter desorption has been shown to be highly unfavorable over long timescales (Gu *et al.*, 1995). Lipids preserved in this way may be more widespread than expected due to the surprising resilience of martian ferrihydrite to short-lived aqueous events, as observed in laboratory simulations (Dehouck *et al.*, 2017).

In cases where ferrihydrite is buried to depths that are shallow enough to retain its stability, the slight increase in temperature would result in the desorption of lipids, rendering them extractable by wet chemistry experiments. This opens a ''preservation window'' for low-temperature ferrihydrite environments, where lipid biosignatures are preserved and are extractable before being oxidized during interactions with the iron oxide substrate.

The degradation of organic matter in magnetite-rich environments is also relevant to a wide variety of martian environments. Short-lived post-diagenetic hydrothermal fluids or events, such as impact-generated hydrothermal systems, can result in temperatures that are high enough to promote the ferrihydrite–magnetite phase transition (Ames *et al.*, 1998;

Table 3. Quantitative Comparisons Between the Preservation Potentials of Different Mars-Analog Environments Based on Kinetic Data

Mars-analog environment	*Key minerals*	*PPF*	*Example locations and references*
Acidic iron-rich deposit	Jarosite, Goethite, Quartz	21.9–114.0	Fernández-Remolar *et al.* (2005); Tan *et al.* (2018); Williams *et al.* (2015b)
Acidic iron-rich deposit with clay component	Jarosite, Goethite, Kaolinite, Quartz	0.2–1.4	Lewis *et al.* (2015); Tan *et al.* (2018)
Circumneutral iron-rich deposit	Ferrihydrite	0.7–0.8	Emerson and Weiss (2004); Parenteau *et al.* (2016); this study

The PPF was calculated by normalizing the time taken for saturated fatty acids to be fully degraded under martian surface conditions to a standard value of 1 ka. The PFF values for acidic deposits are taken from Tan and Sephton (2020).

PPF = preservation potential factor.

Osinski *et al.*, 2013). A similar scenario can occur if a ferrihydrite deposit is buried to sufficient depth, where temperatures can be ≥150°C depending on the circumstances (Borlina *et al.*, 2015). In these cases, ferrihydrite can be transformed to magnetite within an extremely short timeframe (within 72 h). Phase changes can also be caused by the effects of radiative oxidation (Cairns-Smith, 1978; Braterman *et al.*, 1983). As evidenced by the poor preservation potential of magnetite regardless of provenance, these conditions are deleterious to extractable organic matter preservation and should not be considered as sites for future astrobiological missions aimed at using wet chemistry techniques to detect signs of life.

However, magnetite and maghemite derived from the reduction of ferrihydrite could be potential mineralogical biomarkers. Magnetite and/or maghemite formation via this pathway can only occur at elevated temperatures in the presence of water and a reductant such as organic matter. Maghemite has been previously proposed as an astrobiology indicator (Bishop *et al.*, 2008), but these studies drew their conclusions from the heating of synthesized ferrihydrite in the presence of a reducing agent (Campbell *et al.*, 1997; Bishop *et al.*, 2008) rather than the more appropriate aqueous heating of natural terrestrial analogues as is the case in this study.

Although these minerals would contain little diagnostic information about the organic matter (as any organic material would have been consumed as the reductant in this redox reaction), there may be other biogenic signatures associated with the deposit, such as structural biomarkers formed by iron encrustations (Emerson *et al.*, 2010; Williams *et al.*, 2017). Potentially diagnostic insoluble macromolecular organic compounds have been shown to survive simulated diagenesis in iron- and sulfur-rich acid stream environments (Tan *et al.*, 2020); such compounds are likely to survive diagenesis in circumneutral iron-rich deposits as well, and they would be a good target for thermal extraction techniques.

However, it must be emphasized that magnetite found in association with ferrihydrite may have formed via a variety of geochemical pathways that do not require an organic matter reductant; it is now widely accepted that magnetite in the Sheepbed mudstone is formed from the alteration of olivine during the authigenic formation of clay minerals: olivine + Al + oxidizing fluids → saponite + magnetite (McLennan *et al.*, 2014; Vaniman *et al.*, 2014). Magnetite observed in the Murray formation has been interpreted to be the result of the disproportionation of ferrous hydroxide [$Fe(OH)_2$] precipitated under anoxic, alkaline conditions (Schrauzer and Guth, 1976; Hurowitz *et al.*, 2017), or the reduction of ferric iron by dissolved inorganic ferrous-iron complexes (Stumm and Sulzberger, 1992; Hurowitz *et al.*, 2017).

Similarly, maghemite may have been formed by the high-temperature oxidation of magnetite (Cornell and Schwertmann, 2003), the dehydroxylation of lepidocrocite (anhydrous heating at 200°C) (Morris *et al.*, 1998; Cornell and Schwertmann, 2003), the oxidation of Fe(II) complexes in solution (Stumm and Sulzberger, 1992; Cornell and Schwertmann, 2003), the reduction of ferric oxide phases such as ferrihydrite (Cornell and Schwertmann, 2003), or the heating of phosphate-rich ferrihydrite (Barron and Torrent, 2002).

In summary, magnetite and maghemite can be potential mineralogical markers for locations that once contained organic material, especially if there is evidence that they were derived from ferrihydrite precursors and were exposed to elevated temperatures in the presence of water. However, the sheer variety of formative pathways for magnetite and maghemite makes their use as mineralogical biomarkers that are at best limited.

5. Conclusions

Circumneutral, anoxic, iron-rich bogs dominated by ferrihydrite precipitates can support microbial communities in settings that are geochemically, and potentially biologically, similar to Noachian Mars. In this study, we investigated the preservation of lipid biosignatures in one such environment to understand the factors affecting the preservation potential of lipids, as well as organic matter–mineral interactions that underpin the diagenetic processes that control preservation in these environments.

We find that the organic matter–mineral interactions in these iron-rich environments are dominated by the changes in the mineralogy of the iron substrate. As temperature increases, lipids are desorbed from the surface of the ferrihydrite substrate, with peak desorption occurring when ferrihydrite transforms into magnetite, and the surface area of the crystalline iron oxide cannot retain all sorbed material. At the same time, the presence of organic matter was found to influence the transformation products of ferrihydrite; synthetic, organic-poor ferrihydrite was transformed into hematite, whereas natural, organic-rich ferrihydrite inhibited this process and instead transformed into magnetite at higher temperatures. Inorganic–organic interactions showcase the potential for minerals to be indicators of rocks that once contained organic matter; maghemite may be one such residual indicator of an initial mixture of organic matter and iron minerals.

Our results also confirm that saturated fatty acids were the most resistant subset of lipids, consistent with other Mars-analog studies. However, it was also shown that iron-dominated environments are poor targets for wet chemistry-based life detection techniques on Mars, with kinetic modeling indicating that lipids are expected to be completely oxidized on thousand-year timescales, regardless of water availability or specific iron oxide mineralogy.

By comparing our results with previous work, we find that circumneutral iron-rich deposits are less favorable for the preservation of solvent-extractable organic matter compared with other iron-rich deposits, such as acid streams. Future work in which this technique is used will allow us to quantify the relative preservation potential of solvent-extractable organic matter in other Mars-relevant environments and expand the catalogue of potential targets for sample selection strategies on Mars.

Author Disclosure Statement

No competing financial interests exist.

Funding Information

This work was supported by the United Kingdom Space Agency grant ST/N000560/1 and an Imperial College President's PhD scholarship granted to J.T. The code used for kinetic parameter modeling is freely available at: https://www.github.com/ImperialCollegeLondon/ArrheniusModel/blob/master/ChloronapthaleneModellingWork.py

References

Ames DE, Watkinson DH, and Parrish RR (1998) Dating of a regional hydrothermal system induced by the 1850 Ma Sudbury impact event. *Geology* 26:447–450.

Baker BJ and Banfield JF (2003) Microbial communities in acid mine drainage. *FEMS Microbiol Ecol* 44:139–152.

Barron V and Torrent J (2002) Evidence for a simple pathway to maghemite in Earth and Mars soils. *Geochim Cosmochim Acta* 66:2801–2806.

Barrott JJ, Dudeney AWL, and Mason PJ (2014) Spatial and temporal relationships between Eocene sand horizons and iron contamination in stream water in the Thames Basin west of London, UK. *Geochem Explor Environ Anal* 14:33–44.

Bish DL, Blake DF, Vaniman DT, *et al.* (2013) X-ray diffraction results from Mars Science Laboratory: mineralogy of Rocknest at Gale Crater. *Science* 341:1238932

Bishop JL, Dyar MD, Parente M, *et al.* (2006) Understanding surface processes on Mars through study of iron oxides/oxyhydroxides: clues to surface alteration and aqueous processes. *Lunar Planet Sci* XXXVII:4–5.

Bishop JL, Garcia N, Dyar MD, *et al.* (2008) Maghemite as an astrobiology indicator on the Martian surface: reduction of iron oxides by early organic compounds to generate magnetic phases. *Geophys Res Abstr* 10:EGU2008-A-11557.

Blesa MA and Matijević E (1989) Phase transformations of iron oxides, oxohydroxides, and hydrous oxides in aqueous media. *Adv Colloid Interface Sci* 29:173–221.

Booy M and Swaddle TW (1978) Hydrothermal preparation of magnetite from iron chelates. *Can J Chem* 56:402–403.

Borlina CS, Ehlmann BL, and Kite ES (2015) Modeling the thermal and physical evolution of Mount Sharp's sedimentary rocks, Gale Crater, Mars: implications for diagenesis on the MSL Curiosity rover traverse. *J Geophys Res Planets* 120: 1396–1414.

Braterman PS, Cairns-Smith AG, and Sloper RW (1983) Photo-oxidation of hydrated Fe2+-significance for banded iron formations. *Nature* 303:163–164.

Bristow TF, Bish DL, Vaniman DT, *et al.* (2015) The origin and implications of clay minerals from Yellowknife Bay, Gale crater. *Mars Am Mineral* 100:824–836.

Cady SL and Farmer JD (1996) Fossilization processes in siliceous thermal springs: trends in preservation along thermal gradients. *Ciba Found Symp* 202:150–170; discussion 170–173.

Cairns-Smith AG (1978) Precambrian solution photochemistry, inverse segregation, and banded iron formation. *Nature* 276: 807–808.

Campbell AS, Schwertmann U, and Campbell PA (1997) Formation of cubic phases on heating ferrihydrite. *Clay Miner* 32:615–622.

Chan CS, McAllister SM, Leavitt AH, *et al.* (2016) The architecture of iron microbial mats reflects the adaptation of chemolithotrophic iron oxidation in freshwater and marine environments. *Front Microbiol* 7:1–18.

Chyba C and Sagan C (1992) Endogenous production, exogenous delivery and impact-shock synthesis of organic molecules: an inventory for the origins of life. *Nature* 355:125–132.

Cockell CS (2014) Trajectories of martian habitability. *Astrobiology* 14:182–203.

Cockell CS, Schuerger AC, Billi D, *et al.* (2005) Effects of a simulated martian UV flux on the *Cyanobacterium*, *Chroococcidiopsis* sp. 029. *Astrobiology* 5:127–140.

Cornell RM (1979) Influence of organic anions on the crystallization of ferrihydrite. *Clays Clay Miner* 27:402–410.

Cornell RM and Schwertmann U (2003) *The Iron Oxides: Structure, Properties, Reactions, Occurences and Uses*, 2nd ed. Wiley-VCH, Weinheim.

Dartnell LR (2011) Ionizing radiation and life. *Astrobiology* 11: 551–582.

Dartnell LR, Ward JM, and Coates AJ (2007) Martian sub-surface radiation field: biosignatures and geology. *Biogeosciences* 4: 545–558.

Dehouck E, McLennan SM, Sklute EC, *et al.* (2017) Stability and fate of ferrihydrite during episodes of water/rock interactions on early Mars: an experimental approach. *J Geophys Res Planets* 122:1–25.

Duda J-P, Thiel V, Bauersachs T, *et al.* (2018) Ideas and perspectives: hydrothermally driven redistribution and sequestration of early Archaean biomass–the ''hydrothermal pump hypothesis.'' *Biogeosciences* 15:1535–1548.

Eglinton TI and Douglas AG (1988) Quantitative study of biomarker hydrocarbons released from Kerogens during hydrous pyrolysis. *Energy Fuels* 2:81–88.

Eglinton TI, Rowland SJ, Curtis CD, *et al.* (1986) Kerogen-mineral reactions at raised temperatures in the presence of water. *Org Geochem* 10:1041–1052.

Eigenbrode JL, Summons RE, Steele A, *et al.* (2018) Organic matter preserved in 3-billion-year-old mudstones at Gale crater, Mars. *Science* 360:1096–1101.

Emerson D, Fleming EJ, and McBeth JM (2010) Iron-oxidizing bacteria: an environmental and genomic perspective. *Annu Rev Microbiol* 64:561–583.

Emerson D and Weiss JV (2004) Bacterial iron oxidation in circumneutral freshwater habitats: findings from the field and the laboratory. *Geomicrobiol J* 21:405–414.

Farley KA, Malespin C, Mahaffy P, *et al.* (2014) In situ radiometric and exposure age dating of the martian surface. *Science* 343:1247166.

Farmer JD and Des Marais DJ (1999) Exploring for a record of ancient martian life. *J Geophys Res Planets* 104:26977–26995.

Fasiska EJ (1967) Structural aspects of the oxides and oxyhydrates of iron. *Corros Sci* 7:833–839.

Fernández-Remolar DC, Morris RV, Gruener JE, *et al.* (2005) The Rio Tinto Basin, Spain: mineralogy, sedimentary geobiology, and implications for interpretation of outcrop rocks at Meridiani Planum, Mars. *Earth Planet Sci Lett* 240:149–167.

Ferris FG and Magalhaes E (2008) Interfacial energetics of bacterial silicification. *Geomicrobiol J* 25:333–337.

Fleming EJ, Cetinić I, Chan CS, *et al.* (2014) Ecological succession among iron-oxidizing bacteria. *ISME J* 8:804–815.

Fleming EJ, Woyke T, Donatello RA, *et al.* (2018) Insights into the fundamental physiology of the uncultured Fe-oxidizing bacterium *Leptothrix ochracea*. *Appl Environ Microbiol* 84: e02239-17.

Grotzinger JP, Sumner DY, Kah LC, *et al.* (2014) A habitable fluvio-lacustrine environment at Yellowknife Bay, Gale Crater, Mars. *Science* 343:1–14.

Grotzinger JP, Gupta S, Malin MC, *et al.* (2015) Deposition, exhumation, and paleoclimate of an ancient lake deposit, Gale crater, Mars. *Science* 350:aac7575.

Gu B, Schmitt J, Chen Z, *et al.* (1995) Adsorption and desorption of different organic matter fractions on iron oxide. *Geochim Cosmochim Acta* 59:219–229.

Harwood JL and Russel NJ (1984) *Lipids in Plants and Microbes*. George Allen and Unwin, London, United Kingdom.

Hassler DM, Zeitlin C, Wimmer-Schweingruber RF, *et al.* (2014) Mars' surface radiation environment measured with

the Mars Science Laboratory's curiosity rover. *Science* 343: 1244797.

Hoffman N (2001) Modern geothermal gradients on Mars and implications for subsurface liquids. *Conf Geophys Detect Subsurf Water Mars* 53:1689–1699.

Hunt JM, Lewan MD, and Hennet RJC (1991) Modeling oil generation with time-temperature index graphs based on the Arrhenius equation. *Am Assoc Pet Geol Bull* 75:795–807.

Hurowitz JA, Fischer WW, Tosca NJ, *et al.* (2010) Origin of acidic surface waters and the evolution of atmospheric chemistry on early Mars. *Nat Geosci* 3:323–326.

Hurowitz JA, Grotzinger JP, Fischer WW, *et al.* (2017) Redox stratification of an ancient lake in Gale crater, Mars. *Science* 356:eaah6849.

Jaeschke A, Lewan MD, Hopmans EC, *et al.* (2008) Thermal stability of ladderane lipids as determined by hydrous pyrolysis. *Org Geochem* 39:1735–1741.

Kandori K, Kawashima Y, and Ishikawa T (1992) Effects of citrate ions on the formation of monodispersed cubic hematite particles. *J Colloid Interface Sci* 152:284–288.

Killops S and Killops V (2005) *Introduction to Organic Geochemistry*. 2nd ed.: ix +393 pp. Oxford: Blackwell Publishing.

Klein C (2005) Some Precambrian banded iron-formations (BIFs) from around the world: their age, geologic setting, mineralogy, metamorphism, geochemistry, and origin. *Am Mineral* 90: 1473–1499.

Kolattukudy PE and Walton TJ (1972) Structure and biosynthesis of the hydroxy fatty acids of cutin in *Vicia faba* leaves. *Biochemistry* 11:1897–1907.

Konhauser KO, Phoenix VR, Bottrell SH, *et al.* (2001) Microbial-silica interactions in Icelandic hot spring sinter: possible analogues for some Precambrian siliceous stromatolites. *Sedimentology* 48:415–433.

Koopmans MP, Sinninghe Damsté JS, Lewan MD, *et al.* (1995) Thermal stability of thiophene biomarkers as studied by hydrous pyrolysis. *Org Geochem* 23:583–596.

Koopmans MP, Carson FC, Sinninghe Damsté JS, *et al.* (1998) Biomarker generation from Type II-S kerogens in claystone and limestone during hydrous and anhydrous pyrolysis. *Org Geochem* 29:1395–1402.

Lalonde K, Mucci A, Ouellet A, *et al.* (2012) Preservation of organic matter in sediments promoted by iron. *Nature* 483: 198–200.

Leif RN and Simoneit BRT (1995) Confined-pyrolysis as an experimental method for hydrothermal organic synthesis. *Orig Life Evol Biosph* 25:417–429.

Lewan MD (1985) Evaluation of petroleum generation by hydrous pyrolysis experimentation. *Philos Trans R Soc London Ser A Math Phys Sci* 315:123–134.

Lewan MD, Bjorøy M, and Dolcater DL (1986) Effects of thermal maturation on steroid hydrocarbons as determined by hydrous pyrolysis of Phosphoria Retort Shale. *Geochim Cosmochim Acta* 50:1977–1987.

Lewis JMT, Watson JS, Najorka J, *et al.* (2015) Sulfate minerals: a problem for the detection of organic compounds on Mars? *Astrobiology* 15:247–258.

Lovley DR (1991) Dissimilatory Fe(III) and Mn(IV) reduction. *Microbiol Rev* 55:259–287.

McCollom TM and Seewald JS (2006) Carbon isotope composition of organic compounds produced by abiotic synthesis under hydrothermal conditions. *Earth Planet Sci Lett* 243: 74–84.

McLennan SM, Anderson RB, Bell JF, *et al.* (2014) Elemental geochemistry of sedimentary rocks at Yellowknife Bay, Gale Crater, Mars. *Science* 343:1244734.

Michalski JR, Glotch TD, Rogers AD, *et al.* (2019) The geology and astrobiology of McLaughlin Crater, Mars: an ancient lacustrine basin containing turbidites, mudstones and serpentinites. *J Geophys Res Planets* 124:910–940.

Mißbach H, Schmidt BC, Duda JP, *et al.* (2018) Assessing the diversity of lipids formed via Fischer-Tropsch-type reactions. *Org Geochem* 119:110–121.

Montgomery W, Bromiley GD, and Sephton MA (2016) The nature of organic records in impact excavated rocks on Mars. *Sci Rep* 6:1–8.

Morris RV, Golden DC, Shelfer TD, *et al.* (1998) Lepidocrocite to maghemite to hematite: a pathway to magnetic and hematitic Martian soil. *Meteorit Planet Sci* 33:743–751.

Morris RV, Klingelhöfer G, Schröder C, *et al.* (2006a) Mossbauer mineralogy of rock, soil, and dust at Gusev crater, Mars: spirit's journey through weakly altered olivine basalt on the plains and pervasively altered basalt in the Columbia Hills. *J Geophys Res* 111:E02S13.

Morris RV, Klingelhöfer G, Schröder C, *et al.* (2006b) Mössbauer mineralogy of rock, soil, and dust at Meridiani Planum, Mars: opportunity's journey across sulfate-rich outcrop, basaltic sand and dust, and hematite lag deposits. *J Geophys Res* 111:E002791.

Morris RV, Bristow TF, Rampe EB, *et al.* (2019) Mineralogy and formation process for the Vera Rubin Ridge in Gale Crater based on XRD analyses by the CheMin instrument on the MSL rover Curiosity. In *50th Lunar and Planetary Science Conference*. Houston, Texas, p 2132 (Abstract).

Osinski GR, Tornabene LL, Banerjee NR, *et al.* (2013) Impact-generated hydrothermal systems on Earth and Mars. *Icarus* 224:347–363.

Parenteau MN, Jahnke LL, Farmer JD, *et al.* (2014) Production and early preservation of lipid biomarkers in iron hot springs. *Astrobiology* 14:502–521.

Parenteau MN, Jahnke LL, Bristow TF, *et al.* (2016) Preservation of organic compounds in circumneutral iron deposits. In *Biosignature Preservation and Detection in Mars Analog Environments*. Lake Tahoe, Nevada. LPI Contribution No. 1912, id.2076.

Pedersen HD, Postma D, and Jakobsen R (2006) Release of arsenic associated with the reduction and transformation of iron oxides. *Geochim Cosmochim Acta* 70:4116–4129.

Peters KE, Moldowan JM, and Sundararaman P (1990) Effects of hydrous pyrolysis on biomarker thermal maturity parameters: monterey phosphatic and siliceous members. *Org Geochem* 15:249–265.

Phoenix VR, Adams DG, and Konhauser KO (2000) Cyanobacterial viability during hydrothermal biomineralisation. *Chem Geol* 169:329–338.

Potter-McIntyre SL, Chan MA, and McPherson BJ (2014) Textural and mineralogical characteristics of microbial fossils associated with modern and ancient iron (oxyhydr)oxides: terrestrial analogue for sediments in Gale Crater. *Astrobiology* 14:1–14.

Rampe EB, Morris RV, Douglas Archer P, et al. (2016) Recognizing sulfate and phosphate complexes chemisorbed onto nanophase weathering products on Mars using in-situ and remote observations. *Am Mineral* 101:678–689.

Rampe EB, Ming DW, Blake DF, *et al.* (2017) Mineralogy of an ancient lacustrine mudstone succession from the Murray

formation, Gale crater, Mars. *Earth Planet Sci Lett* 471:172–185.

Ratledge C and Wilkinson SG (1988) *Microbial Lipids*, Vol. 1. Academic Press, London.

Royle SH, Tan J, Kounaves SP, *et al.* (2018) Survivability of 1-chloronapthalene during simulated early diagenesis: implications for chlorinated hydrocarbon detection on Mars. *J Geophys Res Planets* 123:2790–2802.

Rush D, Jaeschke A, Geenevasen JAJ, *et al.* (2014) Generation of unusual branched long chain alkanes from hydrous pyrolysis of anammox bacterial biomass. *Org Geochem* 76:136–145.

Schikorr G (1933) About Iron (II) Hydroxide and a Ferromagnetic Iron (III) Hydroxide [German]. *Chemie* 212:33–39.

Schrauzer GN and Guth TD (1976) Hydrogen evolving systems. 1. The formation of H2 from aqueous suspensions of Fe(OH)2 and reactions with reducible substrates, includiing molecular nitrogen. *J Am Chem Soc* 98:3508–3513.

Schwertmann U (1966) Inhibitory effect of soil organic matter on the crystallization of amorphous ferric hydroxide. *Nature* 212:645–646.

Schwertmann U (1970) The influence of simple organic anions on the formation of goethite and hematite from amorphous Fe (III) hydroxide [German]. *Geoderma* 3:207–214.

Sephton MA (2012) Pyrolysis and mass spectrometry studies of meteoritic organic matter. *Mass Spectrom Rev* 31:560–569.

Soliday CL and Kolattukudy PE (1977) Biosynthesis of cutin omega-hydroxylation of fatty acids by a microsomal preparation from germinating *Vicia faba*. *Plant Physiol* 59:1116–1121.

Stumm W and Sulzberger B (1992) The cycling of iron in natural environments: considerations based on laboratory studies of heterogeneous redox processes. *Geochim Cosmochim Acta* 56:3233–3257.

Summons RE, Albrecht P, McDonald G, *et al.* (2008) Molecular biosignatures. In *Strategies of Life Detection*, edited by O Botta, JL Bada, J Gomez-Elvira, E Javaux, F Selsis, and R Summons, Springer US, Boston, MA, pp 133–159.

Sumner DY (2004) Poor preservation potential of organics in Meridiani Planum hematite-bearing sedimentary rocks. *J Geophys Res E Planets* 109:1–8.

Tan J and Sephton MA (2020) Organic records of early life on mars: the role of iron, burial, and kinetics on preservation. *Astrobiology* 20:53–72.

Tan J, Lewis JMT, and Sephton MA (2018) The fate of lipid biosignatures in a Mars-analogue sulfur stream. *Sci Rep* 8:7586.

Tan J, Royle SH, and Sephton MA (2021) Artificial maturation of iron- and sulfur-rich mars analogues: implications for the diagenetic stability of biopolymers and their detection with pyrolysis–gas chromatography–mass spectrometry. *Astrobiology* 21 doi: 10.1089/ast.2019.2211.

Tannenbaum E and Kaplan IR (1985) Low-Mr hydrocarbons generated during hydrous and dry pyrolysis of kerogen. *Nature* 317:708–709.

Treiman AH, Bish DL, Vaniman DT, *et al.* (2016) Mineralogy, provenance, and diagenesis of a potassic basaltic sandstone on Mars: cheMin X-ray diffraction of the Windjana sample (Kimberley area, Gale Crater). *J Geophys Res Planets* 121:75–106.

Vago JL, Westall F, Coates AJ, *et al.* (2016) Habitability on early mars and the search for biosignatures with the ExoMars rover. *Astrobiology* 17:471–510.

Vaniman DT, Bish DL, Ming DW, *et al.* (2014) Mineralogy of a mudstone at Yellowknife Bay, Gale Crater, Mars. *Science* 343:1–9.

Vesenka J, Havu J, Hruby K, *et al.* (2018) A model for sheath formation coupled to motility in *Leptothrix ochracea*. *Geomicrobiol J* 35:366–374.

Westall F, Foucher F, Bost N, *et al.* (2015) Biosignatures on Mars: what, where, and how? Implications for the search for martian life. *Astrobiology* 15:998–1029.

Widdel F, Schnell S, Heising S, *et al.* (1993) Ferrous iron oxdation by anoxygenic phototrophic bacteria. *Nature* 362:834–836.

Wilhelm MB, Davila AF, Eigenbrode JL, *et al.* (2017) Xeropreservation of functionalized lipid biomarkers in hyperarid soils in the Atacama Desert. *Org Geochem* 103:97–104.

Williams AJ, Eigenbrode JL, Floyd MM, *et al.* (2015a) Lipid detection in Fe(III)-dominated samples to prepare for the tetramethyl-ammonium hydroxide (TMAH) wet chemistry experiment on the SAM instrument suite. In: *46th Lunar and Planetary Science Conference*. Houston, Texas, 1814.pdf

Williams AJ, Sumner DY, Alpers CN, *et al.* (2015b) Preserved filamentous microbial biosignatures in the Brick Flat Gossan, Iron Mountain, California. *Astrobiology* 15:637–668.

Williams AJ, Eigenbrode JL, Wilhelm MB, *et al.* (2016) Physical and molecular biosignature preservation in hydrous ferric oxides: implications for detection on Mars with MSL and future missions. In *Biosignature Preservation and Detection in Mars Analog Environments*. Lake Tahoe, Nevada. LPI Contribution No. 1912, id.2015

Williams AJ, Alpers CN, Sumner DY, *et al.* (2017) Filamentous hydrous ferric oxide biosignatures in a pipeline carrying acid mine drainage at iron mountain mine, California. *Geomicrobiol J* 34:193–206.

Address correspondence to:
Jonathan Tan
Department of Earth Science and Engineering
Impacts and Astromaterials Research Centre
Imperial College London
London SW7 2AZ
United Kingdom

E-mail: jonathan.tan12@imperial.ac.uk

Submitted 27 July 2020
Accepted 17 December 2020
Associate Editor: Kathleen Campbell

Abbreviations Used

DI = deionized
EOP = even-over-odd predominance
FeOB = iron-oxidizing bacteria
GC-MS = gas chromatography-mass spectrometry
MSL = Mars Science Laboratory
NF = natural ferrihydrite
NFH = natural ferrihydrite pyrolyzed at high water-to-rock ratios
NFL = natural ferrihydrite pyrolyzed at low water-to-rock ratios
PPF = preservation potential factor
SEM = scanning electron microscopy
SF = synthetic ferrihydrite
XRD = X-ray diffraction